SCIEPublish

Article

The Discovering of Rapid Formation $La(OH)_3$ from LaH_3

Xinyue Zhu [1], Bin Wen [1], Changzeng Fan [1,2,*] and Lifeng Zhang [1,3,*]

[1] State Key Laboratory of Metastable Materials Science and Technology, Yanshan University, Qinhuangdao 066004, China; zhuxiny@stumail.ysu.edu.cn (X.Z.); wenbin@ysu.edu.cn (B.W.)

[2] Hebei Key Lab for Optimizing Metal Product Technology and Performance, Yanshan University, Qinhuangdao 066004, China

[3] School of Mechanical and Materials Engineering, North China University of Technology, Beijing 100144, China

* Corresponding author. E-mail: chzfan@ysu.edu.cn (C.F.); zhanglifeng@ncut.edu.cn (L.Z.)

Received: 27 September 2024; Accepted: 12 November 2024; Available online: 14 November 2024

ABSTRACT: It was found that the single crystal of LaH_3 specimen with $Fm\bar{3}m$ (No.225) will decompose into powders within 24 h, which is later characterized to be $La(OH)_3$ by single crystal X-ray diffraction (SXRD) measurements. The discovery motivates the examination of three possible transition paths by comparing formation enthalpy with first-principles calculations and employing a custom- designed hydrogen detection setup. Furthermore, the most suitable adsorption position of O_2 molecules on the (111) surfaces has been investigated by comparing the adsorption enthalpy from different candidate positions by utilizing first-principles calculations, implying the pivotal role of O_2 molecules played in the rapid formation of $La(OH)_3$ along the optimal transition path.

Keywords: LaH_3; $La(OH)_3$; Single crystal; DFT; Adsorption

© 2024 The authors. This is an open access article under the Creative Commons Attribution 4.0 International License (https://creativecommons.org/licenses/by/4.0/).

1. Introduction

As the first element of the f-block of the periodic table, lanthanum is a very abundant and active element and has been widely studied for its fascinating physical and chemical properties [1]. Lanthanum exists in various compounds such as lanthanum hydride [2–4], lanthanum oxide [5–7] and lanthanum hydroxide [8–10], which possess excellent properties like superconductivity [2], superionic conduction [4], catalysis [5], as well as refining grains in the iron industry [6], adsorption of hazard dyes [10] and phosphate removal from wastewater [11]. For the compounds mentioned above and their corresponding unique properties, the crystal structures often play a pivotal role in tailoring the performances. For instance, Laniel et al. [2] have presented seven lanthanum hydrides synthesized in the range of 50 to 180 GPa by single-crystal X-ray diffractions and DFT calculations for the purpose of guiding the search of candidate high-temperature superconductors. Luo et al. [7] reported four types of hexagonal La_2O_3 with varying degrees of oxygen vacancies and crystal characteristics synthesized by ball milling, finding that these oxygen vacancies influence the photocatalytic degradation of tetracycline. On the contrary, Jonderian et al. [10] found that the native crystalline phase of $La(OH)_3$ remains unaltered and dominant by the azo-dye Congo Red adsorption.

There is also considerable research focused on the transformation between La_2O_3 and $La(OH)_3$ [12–14]. Fleming et al. [12] discovered that the La_2O_3 will rapidly hydroxylate to form stable $La(OH)_3$ when exposed to an open atmosphere. Further study suggest that there exists a intermediate LaO(OH)-type phase involved in the hydroxylation and de hydroxylation process. Hu et al. [13] reported that La_2O_3 nanobelts were obtained when the $La(OH)_3$ nanobelts were calcined in air at 690 °C for 6 h. Very recently, Ismail et al. [14] proposed a five-step decomposition pathway $La(OH)_3$, which is firstly converted into $LaOHCO_3$, followed by $LaOHCO_3 \cdot xH_2O$ ($LaOHCO_3 \cdot yH_2O$), then converted into $La_2O_2CO_3$ and finally into La_2O_3 nanorods through annealing.

This work was prompted by simple observations that a piece of single-crystal LaH_3 transforms into powder during single-crystal X-ray diffraction measurements, and a specimen of LaH_3 on a glass sliderapidly turn into white powders within 24 h. In the remaining sections of the paper, the experimental and computational methods will be briefly introduced, followed by the main results on the crystal structures determination on LaH_3 and $La(OH)_3$, as well as the reaction pathway discrimination by self-designed hydrogen detection approach combined with formation and adsorption

https://doi.org/10.70322/gct.2024.10005

enthalpies calculations within the scheme of density functional theory (DFT) method [15–17]. Finally, the main conclusions will be suggested.

2. Materials and Methods

The fragment of lanthanum hydride used for SXRD diffraction was selected from the factory product as is (more than 99.5% purity, Jiangxi Province,China ,zhongxi Metal Materials Co., Ltd., particle size of 100–200 mesh). The lanthanum hydroxide material used for simulated powder X-ray diffraction (PXRD) measurements was the reaction product after the lanthanum hydride material was exposed to the air for 24 h. During the SXRD measurements, lanthanum hydride was placed on a clean glass sheet, washed the surface impurities with anhydrous ethanol and fixed on a thin glass fiber with glue and mounted on the sample stage. All the SXRD measurements were performed using a four-circle single-crystal X-ray diffractometer (Bruker D8 Venture, Bruker AXS GmbH, Karlsruhe, Germany). The hydron detection was carried out with the hydrogen test tape (DX-2106H, Beijing, China,Nitto), with the detected concentrations as low as 1%.

All DFT-based first-principles calculations were performed using the CASTEP [18] program as integrated in the Materials Studio software(2020 verision). The Perdew-Burke-Ernzerhof (PBE) [19,20] exchange correlation functional with generalized gradient approximation (GGA) is used to describe the interaction between the nucleus and the electron and the interaction potential between the ion, and the valence electron is realized by Norm conserving potential. Periodic boundary conditions are applied, and the wave function of crystals is expanded through the plane wave base set. The plane-wave cut-off energy E_{cut} was selected as 830 eV. It has been tested that the PBE-sol method does not change the result, indicating that the top position is the most stable adsorption site. Spin polarization has not been considered as the system is diamagnetism [2]. The Brillouin region integral was divided into K-point grids according to the Monkhorst-Pack scheme, where the density of K-point grids was set as 2 × 2 × 1. In the structure optimisation process, the convergence standards of force and energy were 0.01 eV/Å and 5 × 10^{-6} eV, which have been performed convergence tests for $La(OH)_3$ system. LaH_3 crystal is adopted as a cubic structure with space group $Fm\bar{3}m$ (No.225). Considering calculation accuracy and efficiency, a 7-layer atomic supercell model is constructed to simulate the surface of LaH_3. The vacuum layer is set to be 15 Å, and the atomic coordinates of the bottom five atomic layers are fixed during construction optimization. The top surface atoms relax together with the adsorbed molecules.

3. Results and Discussion

The lanthanum hydride single crystal sample with a size of 0.09 mm × 0.08 mm × 0.05 mm was selected. The reciprocal diffractions projected along three main directions are shown in Figure 1. It is indexed to be $a = b = c = 5.62$ Å, $\alpha = \beta = \gamma = 90°$. The detailed diffraction information during collection and the structural refinement parameters of the LaH_3 phase are illustrated in Table 1. From Table 1, one can find that $Fm\bar{3}m$ -LaH_3 phase fit the SXRD extremely well with the final R indices of 0.4%. The refined crystal structure of $Fm\bar{3}m$ -LaH_3 is also in accordance with the previous structural model in which the hydrogen atoms occupy the tetrahedral and octahedral interstices [21].

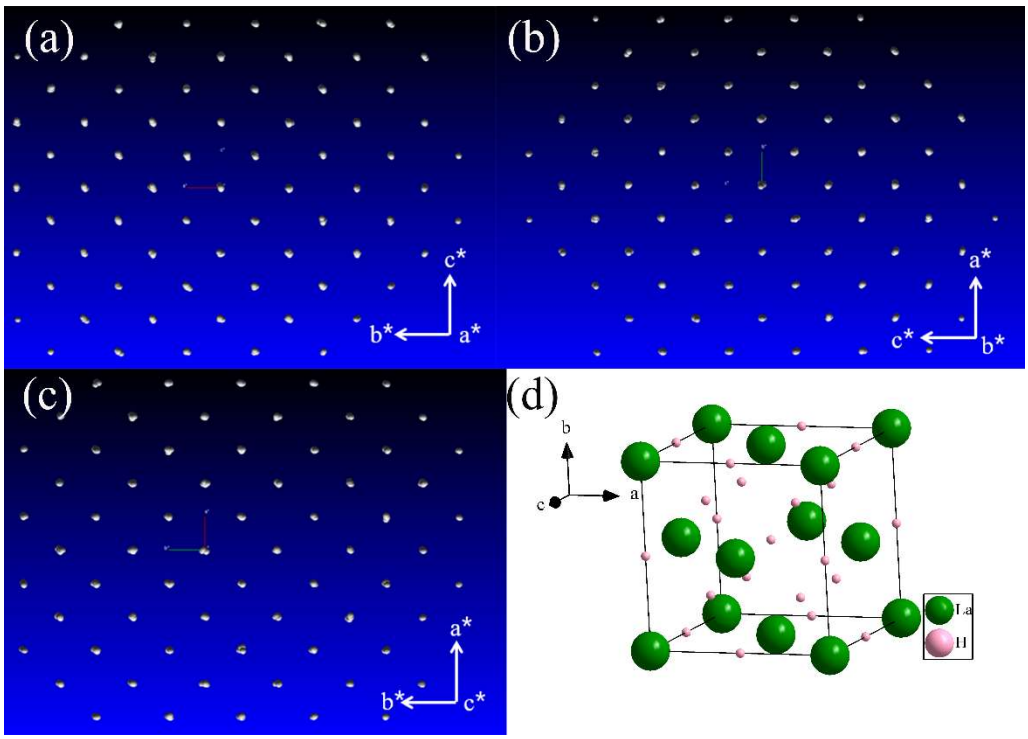

Figure 1. The diffraction patterns projected along (**a**) *a**; (**b**) *b**; (**c**) *c** and (**d**) the crystal structure of LaH_3 phase.

Table 1. Crystallographic and experimental information of LaH_3.

Chemical Formula	**LaH_3**
a, *b*, *c*/Å	5.6151(10), 5.6151(10), 5.6151(10)
α, *β*, *γ*/°	90, 90, 90
V/Å^3	177.04(9)
Z	4
Space group	$Fm\bar{3}m$
Crystal system	Cubic
Diffractometer	Bruker D8 Venture Photon 100 COMS
Monochromator	Graphite
T_{meas}/K	296(2)
Radiation	Mo-K*α*, λ = 0.71073 (Å)
Scan mode	φ and ω scan
Absorption correction	Multi-scan
F(000)	240
θ range/°	6.29~27.15
μ/mm^{-1}	23.50
No. measured reflections	1297
No.unique reflections	22
No. observed reflections (I > 2σ(I))	22
No. reflections used in refinement	22
No. parameters used in refinement	4
Reflection range	$-7 \le h \le 7, -7 \le k \le 7, -7 \le l \le 7$
R_{int}	0.065
R(σ)	0.011
Final R indices ($F_{obs} > 4\sigma(F_{obs})$)	R_1 = 0.0040, ωR_2 = 0.0095
R indices (all data)	R_1 = 0.0040, ωR_2 = 0.0095
Goodness of fit	1.044

The $La(OH)_3$ phase was discovered during SXRD measurements of LaH_3 single-crystal samples.It was found that the LaH_3 sample will change into white powder when exposed to the air within 24 h. The black LaH_3 changes to white $La(OH)_3$, and the density is enhanced significantly after phase transformation (see Figure S1 in the Supplementary Materials). To determine its crystal structure, a piece of white powder measuring 0.2 mm × 0.18 mm × 0.14 mm was selected and mounted on the sample stage of a four-circle single-crystal X-ray diffractometer. A different strategy named the Phi360 test (the sample is rotating around the φ axis for 360°, which is equivalent to PXRD powder diffraction) was adopted for the powder sample. Figure 2a shows the obtained Phi360 diffraction pattern with multiple

Debye rings, indicating that the sample is polycrystalline rather than single-crystalline. The crystallographic information for $La(OH)_3$ is shown in Table 2.

The diffraction peaks were obtained by integrating the Debye rings and compared with the available $La(OH)_3$ standard PDF card, as shown in Figure 2b. The good agreement between PDF#36-1481 and the integrated Debye rings suggests that the phase transition product is primarily $La(OH)_3$, formed from LaH_3 upon exposure to air.The crystal structure model of $La(OH)_3$ is illustrated in Figure 3.

Table 2. Crystallographic and experimental information of $La(OH)_3$.

Chemical Formula	**$La(OH)_3$**
a, *b*, *c*/Å	6.55980, 6.55980, 3.86370
α, *β*, *γ*/°	90, 90, 120
V/Å^3	143.984
Space group	*P*63/*m*
Crystal system	hexagonal

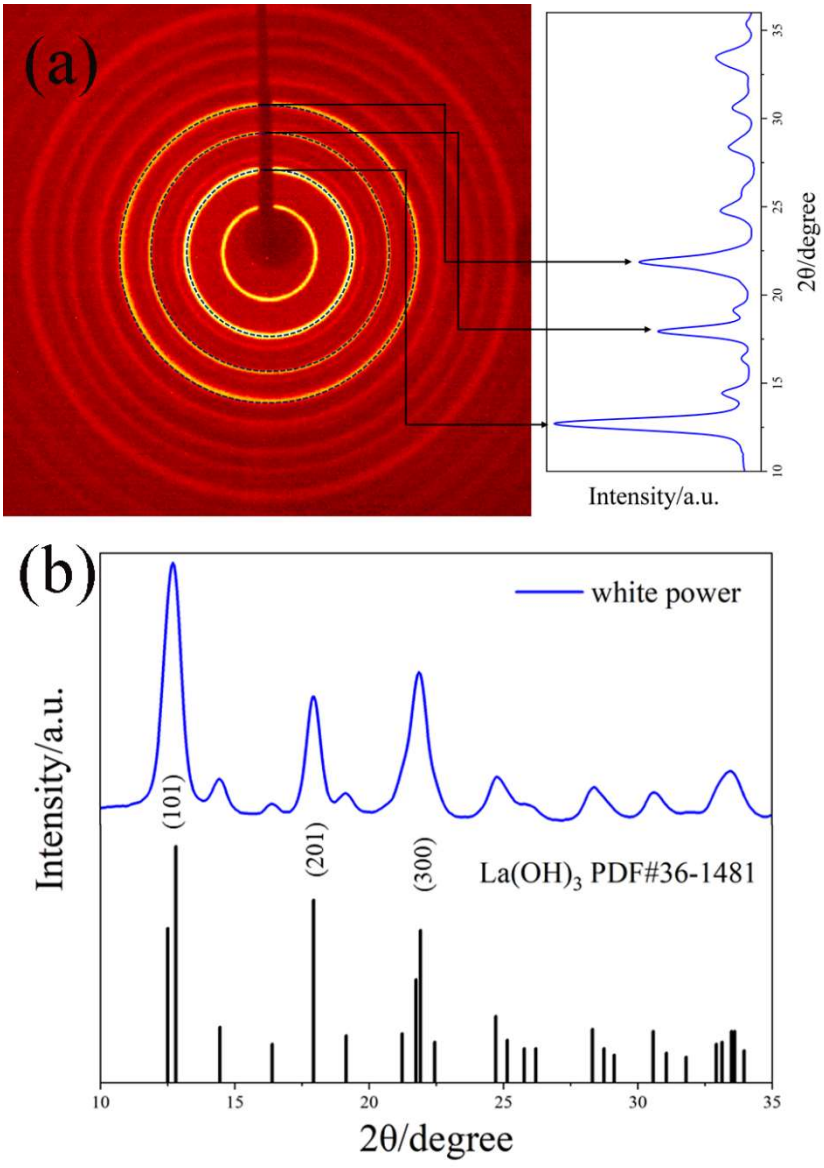

Figure 2. (**a**) phi360 diffraction peak and comparison with (**b**) standard PDF card.

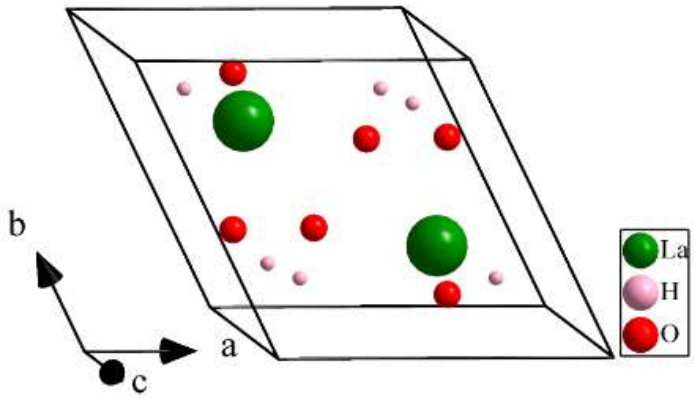

Figure 3. The crystal structure of $La(OH)_3$ phase.

As shown in Figure 4, it was found that the LaH_3 is constructed by tetrahedrons with 9 oxygen atoms centered on one La atom, while $La(OH)_3$ is constructed by octahedrons with 6 H atoms centered on the La atom.

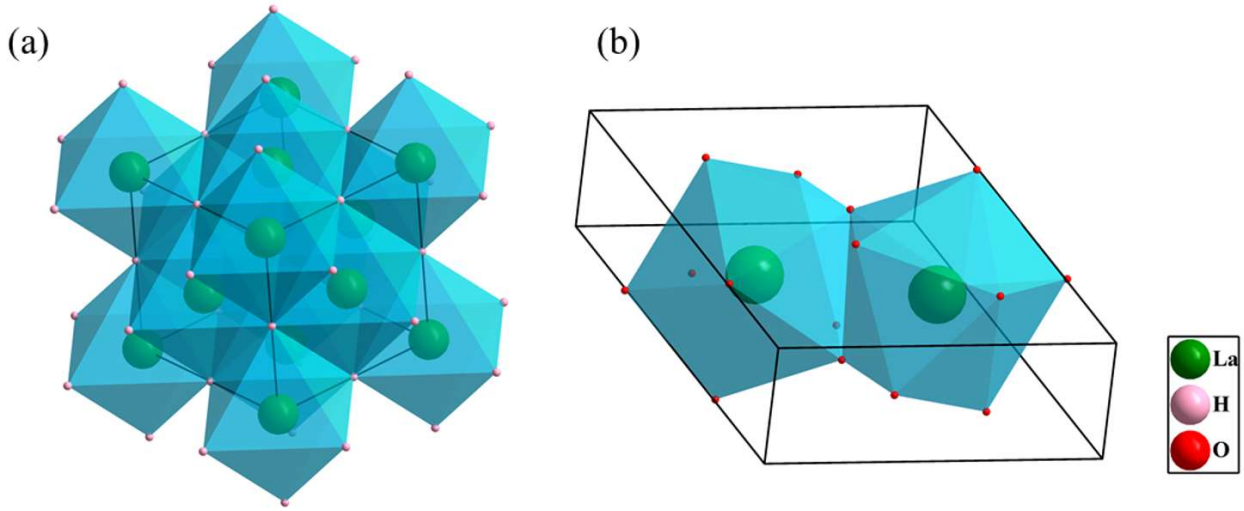

Figure 4. Nanocluster model. (**a**) LaH_3 (**b**) $La(OH)_3$.

Three possible transition paths from LaH_3 to $La(OH)_3$ have been proposed in accordance with the fact that LaH_3 might react with oxygen, or with water vapor, or with both of them:

Reaction route 1:

$$2LaH_3 + 3O_2 \rightarrow 2La(OH)_3 \quad (1)$$

Reaction route 2:

$$LaH_3 + 3H_2O \rightarrow La(OH)_3 + 3H_2 \uparrow \quad (2)$$

Reaction route 3:

$$LaH_3 + O_2 \rightarrow LaOOH + H_2 \uparrow \quad (3)$$

$$LaOOH + H_2O \rightarrow La(OH)_3 \quad (4)$$

In order to discriminate the most suitable reaction route, first-principles calculations have been used to calculate the formation enthalpy of these three reaction routes, as shown in Table 3. Since reaction route 2 has a positive formation enthalpy, it was initially excluded. For the other two reaction routes, route 1 seems more suitable than route 3. However, the possibility of reaction route 3 cannot be excluded extensively. Therefore, a simple hydrogen detection method was designed using special hydrogen detection tape, as shown in Figure 5. The concept is that the tape will change from amber to black if hydrogen gas is produced during reaction route 3, while the container remains partially open to allow

oxygen to participate in the reaction. During our experiment, within 48 h, the tape color remained the original color, as shown in Figure 5. Therefore, the reaction route 3 has also been excluded.

Table 3. Formation enthalpy of three possible reaction routes.

Equation	Formation Enthalpy/eV
1	−15.84
2	+14.58
3	−5.18
4	−0.51

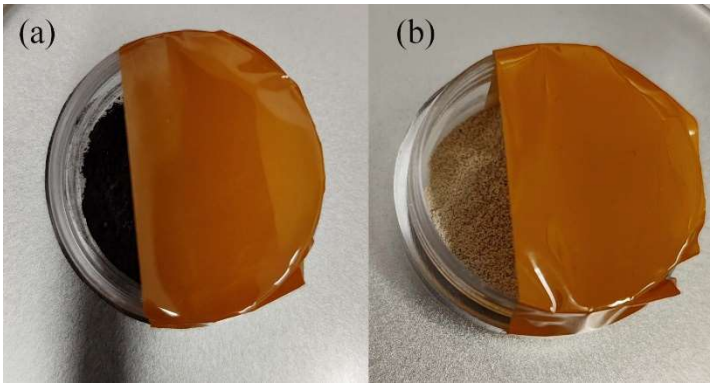

Figure 5. The hydrogen detection experiment (**a**) original state. (**b**) after 48 h.

After the reaction route 1 has been confirmed, first-principles calculations have been utilized to explore the adoption process of oxygen at LaH_3 (100), (110) and (111) surfaces with a hydrogen atom as the plane model by considering the top, bridge and hollow (fcc and hcp) positions.

Surface adsorption energy is adopted to describe the surface adsorption capacity of oxygen molecules. It is the change of total energy caused by the chemical bond reorganization of the whole system after the adsorption of small molecules on a solid surface. The formula is as follows:

$$E_{ads} = E_{total} - E_{surface} - E_{O_2} \quad (5)$$

In the equation, E_{total} is the total energy of the adsorption system, $E_{surface}$ is the total energy of LaH_3 surface structure before adsorption, E_{O_2} is the total energy of spin polarized oxygen molecules in the supercell. The surface adsorption energy can be used to evaluate the adsorption capacity of the surface to oxygen molecules. If the adsorption energy of oxygen molecules is low (i.e., the absolute value of the adsorption energy is high), this indicates a strong adsorption capacity of the surface for oxygen molecules, and vice versa. Surface energy is an important physical quantity for characterizing structural stability and studying the surface of hydrogen storage materials. Surface energy is defined as:

$$E_{surf} = (E_{slab} - NE_{bulk})/2A \quad (6)$$

In the equation, E_{surf} is the energy of the material surface system, E_{slab} is the total energy of the slab model cut in different directions along the cell, N is the number of LaH_3 units in the surface system, E_{bulk} is the total energy of the LaH_3 unit in the cell, A is the system's surface area. The lower the surface energy, the more stable the system.

Table 4 shows the calculated surface energy values of LaH_3's three low exponential surfaces. Obviously, the surface energy of LaH_3's three low exponential surfaces has the following relationship: E_{surf} (100) > E_{surf} (110)> E_{surf} (111). The lowest and most stable surface energy is LaH_3 (111) surface. Therefore, LaH_3 (111) surface is selected as the adsorption surface of oxygen on LaH_3 in the simulation calculation.

Table 4. Surface energy of the low exponential plane of LaH_3.

LaH_3 Surface	2A/m^2	E_{surf}/J·m^{-2}
(100)	1.24×10^{-18}	2.32
(110)	1.76×10^{-18}	1.53
(111)	4.58×10^{-18}	0.86

The adsorption of oxygen molecules on the (111) surface is considered. Figure 6 shows the initial adsorption configuration of the LaH_3 (111) surface, with four highly symmetric adsorption positions: the top position, bridge

position, fcc position, and hcp position. After optimizing the four adsorption sites for the oxygen molecule on the surface, it was found that the top and bridge sites remained unchanged while the other sites shifted. This shows that oxygen molecules have unstable adsorption at the fcc and hcp sites, so the subsequent study only analyzed the adsorption energy at the top and bridge sites. The configurations before and after adsorption of the optimized top and bridge adsorption position have been obtained according to the abovementioned approach and are shown in Figures 7 and 8.

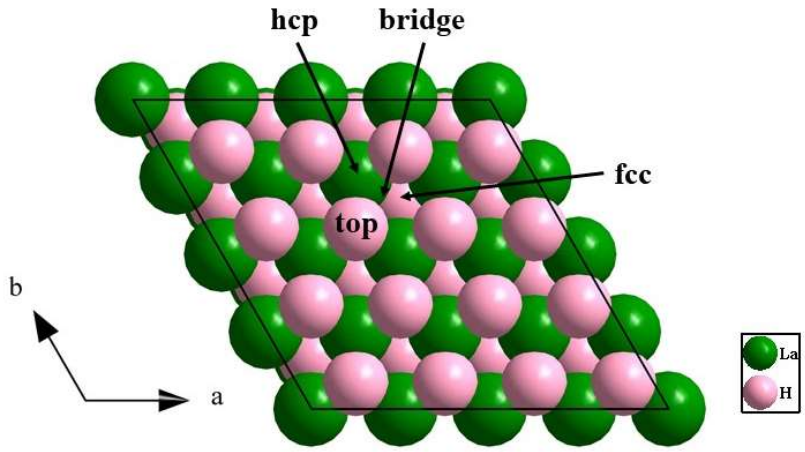

Figure 6. Top view with adsorption position of the (111) surface.

First is the top position of adsorption configuration; after adsorption, O–O bond length increases, tend to have a dissociation and oxygen molecules adsorbed on the surface LaH_3 and with the surrounding La atomic bonding, compared before and after adsorption oxygen molecules and adsorption to the left deviation about 34 degrees. According to the adsorption energy value calculated in Table 5, the top position is the most stable adsorption site for oxygen on the LaH_3 (111) surface.

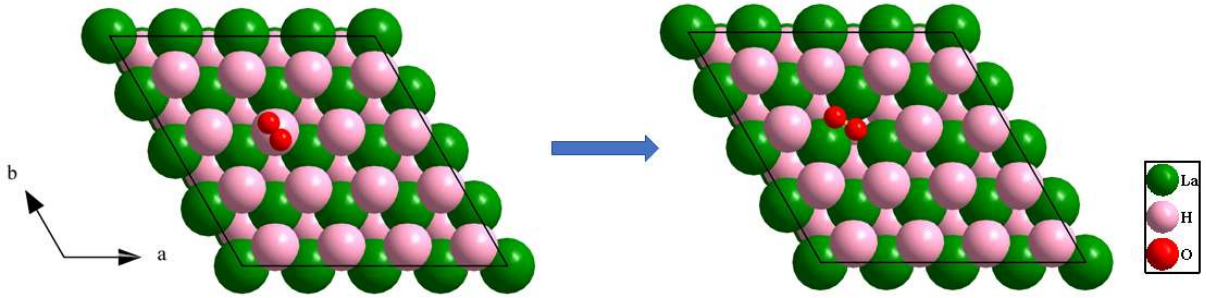

Figure 7. Configuration of (111) surface with top adsorption position before and after geometry optimization.

At the bridge position of adsorption configuration, after adsorption, the length of O-O bond is significantly increased, and the dissociation tendency is greater. Oxygen molecules are adsorbed on the surface of LaH_3 and bond with the surrounding La atoms. The orientation of the oxygen molecules remains unchanged before and after adsorption, and their position shifts closer to the nearby hydrogen atoms.

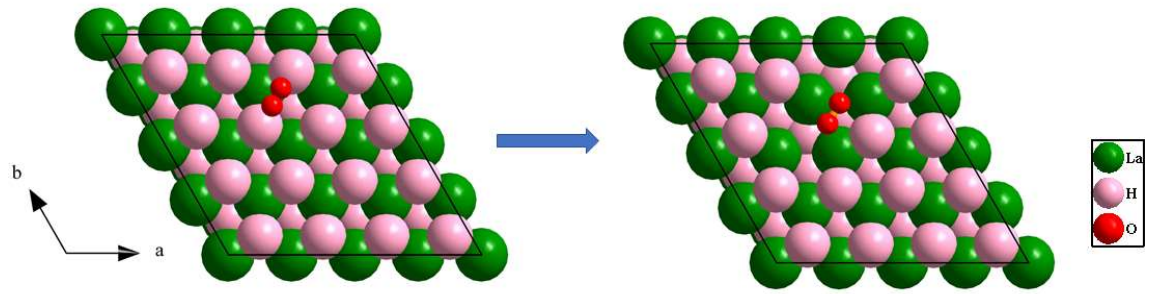

Figure 8. Configuration of (111) surface with bridge adsorption position before and after geometry optimization.

Table 5. Oxygen bond length and adsorption energy after adsorption at each position on the (111) surface.

Position	Length of O-O Bond after Adsorption/Å	Adsorption Energy/eV
top	1.413	−7.66
bridge	1.421	−6.61

4. Conclusions

Motivated by the observations that large-grain of LaH_3 will decompose into powders when exposed to the air within 24 h, both the crystal structures of the LaH_3 and the decomposed product have been solved by SXRD and PXRD, respectively. Meanwhile, the optimal reaction route from LaH_3 to powdered $La(OH)_3$ has been clarified by combining the formation enthalpies and a self-designed hydrogen detection experiment. In addition, the preferred adsorption of oxygen atoms on the (111) surfaces has been extensively investigated by calculating the adsorption energy for all candidate adsorption sites. The conclusions are as follows:

- The LaH_3 single-crystal adopts the cubic structure with space group $Fm\bar{3}m$ (No.225) and lattice constant of $a = b = c = 5.62$ Å, $\alpha = \beta = \gamma = 90°$, agrees well with previous models. The $La(OH)_3$ single crystal adopts a hexagonal structure, the space group is $p63/m$, and the lattice constants are $a = b = 6.56$ Å, $c = 3.86$ Å, $\alpha = \beta = 90°$, and $\gamma = 120°$.
- The decomposed product from LaH_3 is confirmed to be $La(OH)_3$ by comparing the integrating Debye rings from the Phi360 test and comparing with the available standard $La(OH)_3$ PDF card.
- It is clarified that the transformation from LaH_3 to $La(OH)_3$ is primarily driven by the oxidation process of LaH_3. Calculations of the surface energy of LaH_3's three low-index surfaces indicate that the (111) surface is the most stable. By studying the adsorption properties of oxygen on the LaH_3 (111) surface, it is found that the top position is the most stable adsorption position.

Supplementary Materials

The following supporting information can be found at: https://www.sciepublish.com/article/pii/336, Figure S1: Morphology of the sample before and after the phase transition.

Author Contributions

Conceptualization, C.F. and L.Z.; Investigation, X.Z., B.W., C.F. and L.Z.; Writing—Original Draft Preparation, X.Z.; Writing—Review & Editing, C.F., B.W. and L.Z.; Supervision, C.F.; Funding Acquisition, C.F. and B.W.

Ethics Statement

Not applicable.

Informed Consent Statement

Not applicable.

Funding

The National Natural Science Foundation of China (grant No. 52173231; grant No. 51925105); Hebei Natural Science Foundation (grant No. E2022203182); The Innovation Ability Promotion Project of Hebei supported by Hebei Key Lab for Optimizing Metal Product Technology and Performance (grant No. 22567609H).

Declaration of Competing Interest

The authors declare that they have no known competing financial interests or personal relationships that could have appeared to influence the work reported in this paper.

References

1. Mattocks JA, Cotruvo JA, Jr. Biological, biomolecular, and bio-inspired strategies for detection, extraction, and separations of lanthanides and actinides. *Chem. Soc. Rev*. **2020**, *49*, 8315–8334.

2. Liu HY, Naumov II, Hoffmann R, Ashcroft NW, Hemley RJ. Potential high-Tc superconducting lanthanum and yttrium hydrides at high pressure. *Proc*. *Natl. Acad. Sci. USA* **2017**, *114*, 6990–6995.
3. Laniel D, Trybel F, Winkler B, Knoop F, Fedotenko T, Khandarkhaeva S, et al. High-pressure synthesis of seven lanthanum hydrides with a significant variability of hydrogen content. *Nat. Commun*. **2022**, *13*, 6987.
4. Zhang WJ, Cui JR, Wang SS, Gao HJ, Wu AN, Xia YH, et al. Deforming lanthanum trihydride for superionic conduction. *Nature* **2023**, *616*, 73–76.
5. Gangwar BP, Palakollu VP, Singh A, Kanvah S, Sharma S. Combustion synthesized La_2O_3 and $La(OH)_3$: Recyclable catalytic activity towards Knoevenagel and Hantzsch reactions. *RSC. Adv*. **2014**, *4*, 55407.
6. Jiao XY, Fu WT, Shao W, Zhu XW, Zhou YF, Xing XL, et al. First-principles calculation on γ-Fe/La_2O_3 interface properties and austenite refinement mechanism by La_2O_3. *Mat. Chem. Phys*. **2021**, *259*, 124194.
7. Luo XW, Xu L, Yang LB, Zhao JW, Asefa T, Qiu RL, et al. Ball Milling of La_2O_3 Tailors the Crystal Structure, Reactive Oxygen Species, and Free Radical and Non-Free Radical Photocatalytic Pathways. *ACS Appl. Mater. Interfaces* **2024**, *16*, 18671–18685.
8. Huang WY, Li D, Liu ZQ, Tao Q, Zhu Y, Yang J, et al. Kinetics, isotherm, thermodynamic, and adsorption mechanism studies of $La(OH)_3$-modified exfoliated vermiculites as highly efficient phosphate adsorbents. *Chem. Eng. J.* **2014**, *236*, 191–201.
9. Malka T, Zhang XD, Wachtel E, Guo X, Lubomirsky I, Ehre D. Electrical conductivity of lanthanum hydroxide below 473 K. *Solid State Ion.* **2022**, *386*, 116027.
10. Jonderian A, Ammar M, El-Rassy H, Al-Ghoul M. Combined experimental and DFT study on the adsorption of congo red dye using self-assembled hierarchical microspheres of lanthanum hydroxide. *Colloids Surf. A* **2024**, *681*, 132728.
11. Lu YY, Wang H, Chang RR, Li WB, Huang BC, Jin RC. A literature review on phosphate removal from wastewater by lanthanum-based adsorbents: From mechanisms to applications. *J. Water Process Eng*. **2024**, *61*, 105282.
12. Fleming P, Farrell RA, Holmes JD, Morris MA. The Rapid Formation of $La(OH)_3$ from La_2O_3 Powders on Exposureto Water Vapor. *J. Am. Ceram. Soc*. **2010**, *93*, 1187–1194.
13. Hu CG, Liu H, Dong WT, Zhang YY, Bao G, Lao CS, et al. $La(OH)_3$ and La_2O_3 Nanobelts—Synthesis and Physical Properties. *Adv. Mater*. **2007**, *19*, 470–474.
14. Ismail W, Belal A, Abdo W, EI-Shaer A. Investigating the physical and electrical properties of La_2O_3 via annealing of $La(OH)_3$. *Sci. Rep*. **2024**, *14*, 7716.
15. Ren Y, Liu XJ, Tan X, Sun SY, Wei H, Lu F. Adsorption and pathways of single atomistic processes on NbN (0 0 1) and (1 1 1) surfaces: A first-principle study. *Appl. Surf. Sci*. **2014**, *298*, 236–242.
16. Chen JH, Chen Y, Long XH, Li YQ. DFT study of coadsorption of water and oxygen on galena (PbS) surface: An insight into the oxidation mechanism of galena. *Appl. Surf. Sci*. **2017**, *420*, 714–719.
17. Cheng CY, Xie W, Li HJ, Fu QG. Oxygen adsorption on ideal ZrB_2 and ZrC surfaces. *J. Alloys Compd*. **2020**, *830*, 154655.
18. Segall MD, Lindan PJD, Probert MJ, Pickard CJ, Hasnip PJ, Clark SJ, et al. First-principles simulation: Ideas, illustrations and the CASTEP code. *J. Phys Condens. Mat.* **2002**, *14*, 2717.
19. Milman V, Winkler B, White JA, Pickard CJ, Payne MC, Akhmatskaya EV, et al. Electronic structure, properties, and phase stability of inorganic crystals: A pseudopotential plane-wave study. *Int. J. Quantum Chem*. **2000**, *77*, 895–910.
20. Perdew JP, Burke K, Ernzerhof M. Generalized gradient approximation made simple. *Phys. Rev. Lett*. **1996**, *77*, 3865.
21. Yamoyuki T, Iimura S, Kim J, Hosono H. Extremely Shallow Valence Band in Lanthanum Trihydride. *J. Am. Chem. Soc*. **2023**, *145*, 560–566.